Lateral excitonic switching in vertically stacked quantum dots

Jarosław R. Jarzynka,[1] Peter G. McDonald,[1] John Shumway,[2,a)] and Ian Galbraith[1]
[1]*Institute of Photonics and Quantum Sciences, SUPA, School of Engineering and Physical Sciences, Heriot-Watt University, Edinburgh EH14 4AS, United Kingdom*
[2]*Department of Physics, Arizona State University, Tempe, Arizona 85287, USA*

(Received 1 December 2015; accepted 25 May 2016; published online 13 June 2016)

We show that the application of a vertical electric field to the Coulomb interacting system in stacked quantum dots leads to a 90° in-plane switching of charge probability distribution in contrast to a single dot, where no such switching exists. Results are obtained using path integral quantum Monte Carlo with realistic dot geometry, alloy composition, and piezo-electric potential profiles. The origin of the switching lies in the strain interactions between the stacked dots hence the need for more than one layer of dots. The lateral polarization and electric field dependence of the radiative lifetimes of the excitonic switch are also discussed. *Published by AIP Publishing.*
[http://dx.doi.org/10.1063/1.4953391]

I. INTRODUCTION

Even the simplest circuits need a switch to stop, start, or redirect the flow of current, photons, or bits. Switching the state of a system by interaction of the matter with a single photon or the external fields opens new possible applications in measurements[1] and quantum computing.[2] Switches based on an electron-hole pair system (exciton) have been successfully realized in coupled quantum wells and implemented into an exciton optoelectronic transistor, excitonic bridge, or pinch-off modulator.[3] A similar type of excitonic switch can be successfully realized and controlled in a multiple quantum dot system, which opens up new possibilities for solid-state based quantum communication devices[4–6] and quantum memory cells.[7]

Self-assembled vertically coupled dots are also excellent candidates for switching. Their complex piezoelectric field interacting with confinement potentials and external electric fields allows the control of the heavy-hole (HH) exciton charge distribution. The introduction of periodic elongation in the vertical direction additionally permits the access to light-hole (LH) states, which opens the way to dynamic switching not only in the plane of the dots but also between HH and LH excitons.[8] A further advantage is the small size of the device which allows for very dense packaging of the detecting or emitting structures. Currently, we are approaching the regime where electronic properties of few particle states govern device operations via the interaction with confining potentials, strain, Coulomb forces, and external fields.[9] Such low-dimension electronic systems characterized by modified densities of states enable the development of novel devices with optimized performance, e.g., quantum dot lasers,[10,11] or light emitters in qubits for quantum computation devices.[12]

In this article, we report a novel exciton-based switch, theoretically realized in coupled quantum dots using Path Integral Quantum Monte Carlo (PI-QMC) simulations. In contrast to a single InGaAs quantum ring where lateral switching is seen,[13] in a single quantum dot no lateral switching is observed. However, for coupled dots, as we show here, the piezoelectric landscape supports lateral switching.

The impact of the electric field (parallel to the growth direction) on exciton emission spectra is investigated and used to determine the lateral switching of the exciton charge distribution and the intrinsic dipole moment in the coupled dots. Switching of the probability density of the electron-hole pair in the plane perpendicular to the applied electric field and switching of the built-in dipole moment allow insight into the relative localization of charge carriers in the semiconductor nanostructure. This will play a significant role when new devices assembled from densely packed interacting quantum structures are designed.

The article has the following structure: in Section II, the details of the atomistic strain model of the considered nanostructure are discussed. The PI-QMC method is outlined in Section III. Results are presented in Section IV, and physics of the stacked quantum dot excitonic switch is explained.

II. QUANTUM DOT MODEL

The switching effect we report arises from the interaction of the two-body excitonic state with piezoelectric fields in the strained GaAs layers between dots. To perform a quantitative study of the switching effect, it is necessary to have a numerical technique that includes both detailed modeling of the materials' properties of the dots and accurately solves for the correlated two-body excitonic state. We use an atomistic model of the self-assembled dots to accurately model the strain fields. Strain-modified band offsets are used to construct a detailed, three-dimensional effective mass Hamiltonian for the electron and hole.

The model of the quantum dot used is shown in Fig. 1. The single structure Fig. 1(a) is a 4-nm-tall $In_{0.5}Ga_{0.5}As$ truncated-conical dot of a base radius 10.2 nm and top radius 7.2 nm, located on a 0.9 nm thick $In_{0.3}Ga_{0.7}As$ wetting layer. A typical simulation contains approximately 1.7×10^7 atoms placed in a random alloy structure as described in Ref. 14

[a)]Current address: Stone Ridge Technology, Bel Air, MD 21014, USA.

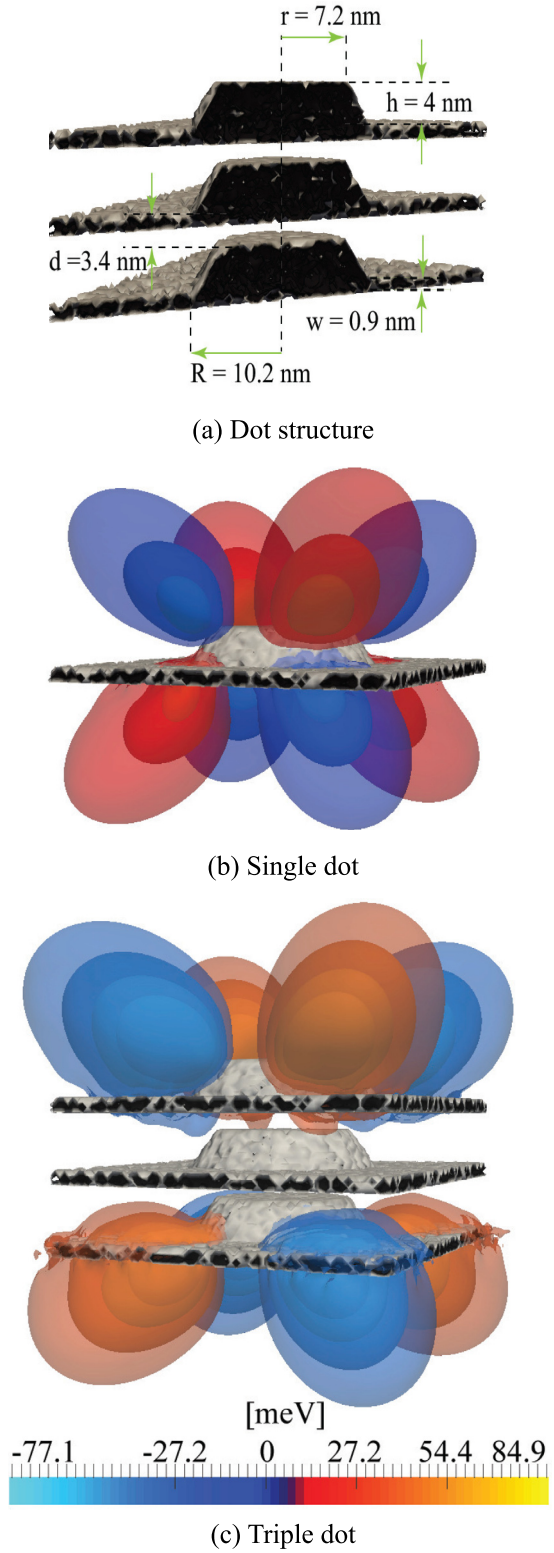

FIG. 1. Cross-section of model quantum dots with piezoelectric potentials of truncated-conical dot. The calculated piezoelectric potential iso-surfaces are also shown.

and immersed in a GaAs matrix. The triple dot system, Fig. 1(c), is formed by stacking single structures in the vertical direction with a separation a 3.4 nm between the top and bottom of the adjacent dots. The figure also shows iso-surfaces of the piezo-electric fields in the strained GaAs matrix surrounding the dots. Triple dot structures have been simulated in a similar fashion.

Lattice mismatch strain generates strong induced piezoelectric potentials. The valence force field method (VFF)[15] is used to relax the atoms from their initial zinc-blende lattice distribution to their equilibrium positions, and the resulting relaxed positions and residual forces are then used to compute the stress tensor for grid. The contribution to the stress tensor is calculated for each atom from the VFF potentials. We approximate the local strain field from the stress tensor averaged over eight-atom cubic cells and bulk elastic constants.[16] The piezo-electric fields are then calculated from the strain field including both linear and non-linear terms[17]

$$p_\mu = \sum_{i=1}^{6} e_{\mu i}\eta_i + \frac{1}{2}\sum_{i,k=1}^{6} B_{\mu ik}\eta_i\eta_k, \qquad (1)$$

where $e_{\mu i}$ is the third-rank proper piezoelectric tensor of the unstrained compound, $B_{\mu ik}$ describes the first-order change of the piezoelectric tensor due to strain, and η_i represents six independent components of the strain tensor (in the Voigt notation).[17] We calculate the piezoelectric charge densities by taking the divergence of these fields, and then calculate the resulting piezoelectric potential, Φ_{pz}. While detailed comparisons are hard to make given the number of material parameters involved, the piezoelectric potentials thus obtained are in good agreement with the analytic approach of Davies.[18]

Typical piezo-electric potentials for single and triple dots are shown in Fig. 1, and these, as will be shown, significantly perturb the electronic states in the structure. The strong piezo-electric field in the GaAs barrier region is also crucial to the lateral switching operation.

Electrons and holes experience different confining potentials in the [110] and $[1\bar{1}0]$ directions. Similarly, in coupled structures confinement varies not only on two perpendicular diagonals but also from dot to dot. In Fig. 2, the valence band profile across the single and triple dots structure is plotted. The LH energy calculated from the biaxial strain shift is also indicated and compared to the ground and first excited state of the HH in the single and triple nanostructure.

For clarity, the lateral confinement potential in Fig. 2 is averaged over the vertical extent and over [110] and $[1\bar{1}0]$ directions. In the single dot, the mean value on two diagonals is plotted. It is evident that in the triple dot the biaxial strain drives the LH states towards the bottom of potential well. In the single structure, the impact of the LH is also weakened as the LH branch is localized in the surrounding matrix away from the dot. It is worth mentioning that in both types of structures, the spin-orbit splitting energy band $\Delta = 0.3\,\text{eV}$ (Ref. 19) greatly exceeds the range of confining potential and similarly to the LH branch, do not affect our calculations. We conclude, in agreement with Refs. 7 and 8 that the HH exciton dominates in InGaAs dot structures.

In order to illustrate the profile of the valence and conduction band in the single and triple quantum structure, the band profile is plotted in the growth direction [001] along the axis of the dot in the inset to Fig. 2

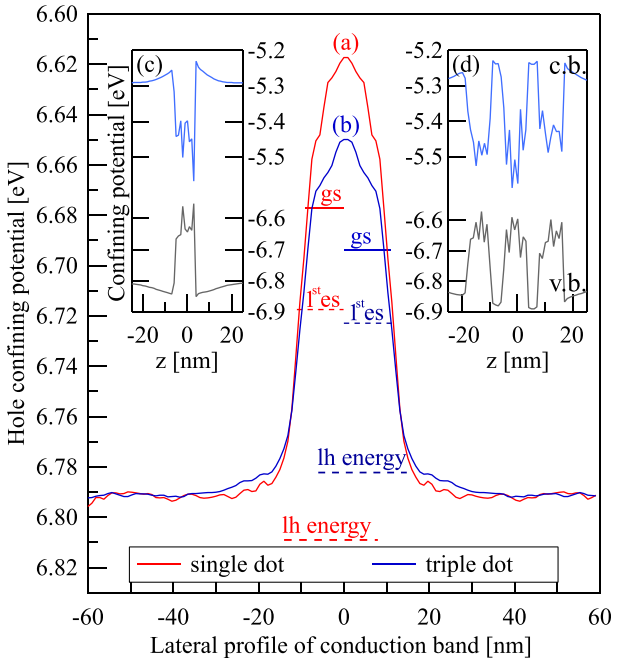

FIG. 2. Lateral valence band profile of (a) single dot and (b) triple dot structures averaged over the vertical extent, and over [110] and [1$\bar{1}$0] directions. Also indicated are the ground state (gs) and the first excited state (1st es) of the single particle heavy-hole in the single and vertically stacked structure. Insets show (c) single dot and (d) triple dot conduction (c.b.) and valence band (v.b.) profile in the growth direction along the axis of the dot.

These confining and piezoelectric potentials are used in a two-band effective mass Hamiltonian

$$H = \frac{p_h^2}{2m_h^*} + \frac{p_e^2}{2m_e^*} + V_h(\mathbf{r}_h) + V_e(\mathbf{r}_e) - \frac{e^2}{4\pi\epsilon_0\epsilon_r|\mathbf{r}_{eh}|} + e\Phi_{\rm pz}(\mathbf{r}_e) - e\Phi_{\rm pz}(\mathbf{r}_h) - e\boldsymbol{E}\cdot\mathbf{r}_{eh}, \quad (2)$$

where the effective masses are $m_e = 0.067\,m_e$ and $m_h = 0.144\,m_e$, $\mathbf{r}_{eh} = \mathbf{r}_e - \mathbf{r}_h$ and the dielectric constant $\epsilon_r = 12.5$. The uniform external electric field, $\boldsymbol{E}$, is used to drive the excitonic switching.

III. THE PATH INTEGRAL METHOD

The switching behavior relies on (i) the details of the three dimensional geometry, (ii) the strong piezoelectric fields inside and outside the dots, and (iii) electron-hole correlation from strong electron-hole Coulomb interaction. The PI-QMC method allows an essentially exact treatment of the model Hamiltonian, Eq. (2). As there is no basis-set expansion or trial-wavefunction needed, shifting of the quantum state between dots and in the inter-dot barrier region, and the cusp as the electron and hole approach each other are all represented without variational or basis-set bias. This allows an accurate prediction of experimentally observable excitonic polarizabilites and radiative recombination rates, quantities which are known to require treatment of quantum correlations.

The essence of the PI-QMC method is to write the excitonic thermal-density matrix as a path integral

$$\rho(\mathbf{r}_e\,\mathbf{r}_h, \mathbf{r}'_e\,\mathbf{r}'_h; \beta) = \frac{1}{Z}\int_{\substack{\mathbf{R}(0)=\{\mathbf{r}'_e,\mathbf{r}'_h\}\\ \mathbf{R}(\beta\hbar)=\{\mathbf{r}_e,\mathbf{r}_h\}}} \mathcal{D}\mathbf{R}(\tau)e^{-S_E[\mathbf{R}(\tau)]/\hbar}, \quad (3)$$

where $\mathbf{R}(\tau)$ is the imaginary-time trajectory of the electron and hole, S_E is the Euclidian action for the model Hamiltonian, Eq. (2), and $\beta = 1/k_bT$ with temperature T. This path integral is evaluated with Monte Carlo sampling as described in Ref. 16. We perform the calculations at a low temperature (12 K) so that the thermal density matrix describes the ground state excitonic wavefunction.

A. Calculation of exciton energy, probability density, and pair correlation functions

Properties of the excitonic wavefunction are calculated from the thermal density matrix as the path integral is sampled. We give a brief description here, and further details can be found in Ref. 16.

The energy is calculated from the thermodynamic energy estimator, $E = -(1/Z)(dZ/d\beta)$. Potential energy contributions arise from the physical location of the electron and hole trajectory. Kinetic energy contributions come from quantum confinement, the extent to which the confining potential and Coulomb forces prevent the trajectories from extending as much as they would for free particles.

The probability density and pair correlation functions can be calculated directly from the electron and hole trajectories in imaginary time. This is very similar to how the quantities would be calculated in a classical simulation, yet the path integral includes all quantum confinement and quantum correlation effects. This intuitive aspect of path integrals is particularly appealing for studies of quantum nanostructures.

B. Calculating polarizability

The effect of an external electric field may be treated by the direct inclusion of an electric field in the Hamiltonian, in which case energies, charge densities, pair correlation functions, and radiative rates may be collected as a function of applied electric field. There are two difficulties with the direct application of an electric field. First, a separate PI-QMC calculation must be performed for each electric field choice. Second, the estimation of the polarizability requires an accurate calculation of the total energy of the exciton, since the polarizability is the quadratic dependence of the recombination energy with the applied field.

Linear response theory may also be used to compute polarizabilites of exciton in the presence of modest electric fields.[17,20] In the linear response theory, the polarizability is given by the imaginary-time fluctuation of the electron-hole dipole moment. This allows the polarizability tensor to be calculated from a single PI-QMC simulation without an applied field. Further, the linear response theory uses the electric dipole moment, which has much less Monte Carlo noise than energy differences, allowing a faster determination of accurate polarizabilites. One limitation of the linear-repose theory is that it may miss non-linear effects of stronger electric fields.

In this work, we combine both approaches. We explicitly include the strong vertical ([001]) electric fields that drive the switching. This is important because the interesting switching behavior is non-linear. This also allows us to calculate charge densities, pair correlation functions, and radiative recombination rates as a function of the vertical field strength. For comparison to experiments, we also calculate the lateral polarizability of the exciton in its two different switched states. We use dipole-dipole fluctuations and the linear response theory to calculate the lateral polarizability. Thus, we obtain the response of the exciton to a weak, probing electric field as for a range of strong vertical fields.

C. Calculating radiative recombination rates

We calculate radiative recombination rates as described in Ref. 14. The mathematical formalism follows directly from Fermi's golden rule for spontaneous photon emission. For excitonic recombination in quantum dots, there are two physical aspects to the radiative recombination rate: (1) the electron and hole must meet each other to recombine, and (2) quantum coherence of the electron-hole contact across a large volume enhances the radiative recombination. The first consideration leads to larger rates when the electron and hole have higher overlap, for example, in a small dot, or because of strong electron-hole correlation. The second consideration leads to larger rates if electron-hole correlation allows the exciton to maintain coherence across a larger nanostructure. For the present stacked-dot geometry with external fields, the asymmetry of the electron and hole confining potential diminishes the second effect, so radiative recombination rates are primarily affected by the amount of electron-hole contact in the wavefunction.

The radiative rate is sampled by allowing the path integral, Eq. (3), to include two configurations: (1) a direct contribution with closed electron-hole paths that samples the trace of the density matrix, and (2) a radiating contribution where the electron and hole connect at a single point at imaginary times $\tau = 0$ and $\tau = \beta\hbar$. The rate follows directly from the ratio the path integral for the two configurations. Further details of the radiative recombination rate calculations are given in Ref. 14.

IV. RESULTS

We begin with a discussion of the charge distribution in a single-dot structure, with and without an applied electric field. Next, we discuss the switching effect in the triple-dot structure, which is much richer due to both the additional vertical structure as well as the strong piezoelectric fields between the dots. To gain further insights into the switching, we show pair correlation functions for the excitonic states in single and triple dots, as a function of applied electric field. We have also completed calculations for double dots (not shown) whose behavior is found to lie between those of the single and triple dots described below. Finally, we present calculations of radiative recombination rates for the correlated excitonic states.

A. Charge distribution in single and stacked dots

The simplest way to understand the switching behavior in stacked dots is to visualize at the charge distributions of the electron and hole. As will be shown, for single dots, these charge distributions are unremarkable and serve as a baseline for the absence of switching. For stacked dots, the charge distributions are interesting in both the vertical and lateral distribution. The switching behavior can be seen as a 90° rotation of the lateral charge density, driven by a vertical applied field.

1. Charge distribution in single dots: Absence of switching

Electrons and holes are subject to different confining potentials in the growth direction, Figs. 3(a) and 3(b). This results in a spatial separation of electrons and holes producing a permanent dipole moment.[21–24] The dipole couples to any external electric field, which will pull(push) the electron-hole system apart(together) in the vertical direction and affects its oscillator strength. The size of the dipole depends strongly on the dot composition profile, in particular, on the In concentration.[25]

We theoretically study the influence of two opposite orientations of a static electric field, E, along the growth direction on the bound states in the quantum dot.

The slice through the center of a single dot in the $[1\bar{1}0]$ direction, Figs. 4(g)–4(i), shows the charge density profile of the heavy-hole exciton as a function of the applied field. It can be seen that the quantum dot has a small inverted (electron-over-hole) dipole with 0 kV/cm applied electric field. The wider lateral confinement near the bottom of the conical pyramid is more effective in localizing the heavy hole than the light electron, inducing this small dipole. Stronger dipoles induced

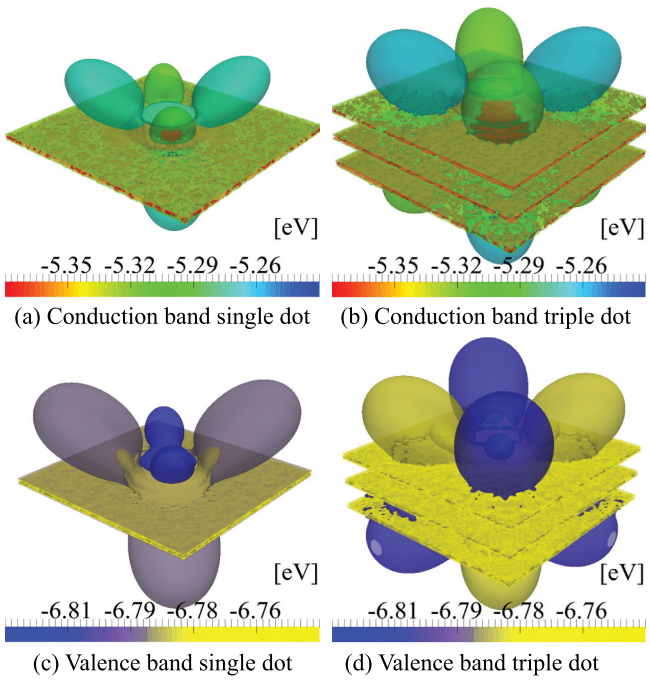

FIG. 3. Strain and piezoelectric field modified conduction and valence band the model quantum dots.

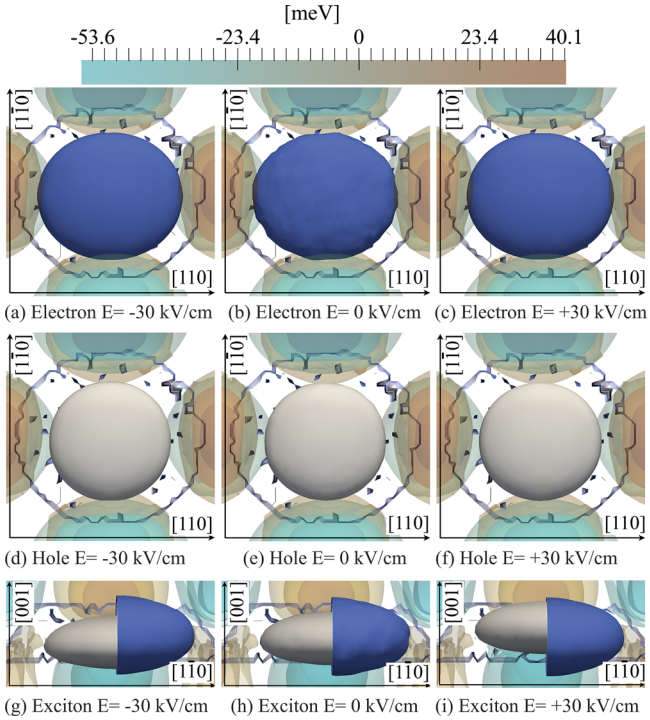

FIG. 4. Single quantum dot. Volumetric cross-section of electron and hole charge distributions with and without the applied vertical ([001]) electric field. We include isosurfaces of the piezoelectric potential and the outline of the quantum dot structure. In panels (a)–(f), the horizontal extent corresponds to the [110] direction and the vertical one to the $[1\bar{1}0]$ direction. In panels (g)–(i), the height of picture represents the [001] direction and the width $[1\bar{1}0]$ direction, and for clarity the hole isosurface is shown on the left (grey) and electron isosurface on the right (blue).

by In gradients and the resulting strain profiles are well-known.[25] The piezoelectric potential adds to the strain fields and perturbs the valence band which enhances localization of the hole wave function in the [110] direction, Fig. 3(c). The conduction band is only weakly affected by biaxial strain, allowing the electron charge distribution to be delocalized in the structure and even tunnel into the barrier material. The piezoelectric potential interacts with conduction band, but as shown in Fig. 3(a) the minima are shallower and appear to not directly overlap with the confining potential in the structure. The vertical electric field applied to the system stretches the electron-hole pair, reducing the exciton binding energy. The orientation of the electric field has also a significant impact on the polarity of the exciton in the quantum dot as shown in Figs. 4(g) and 4(i). In the lateral direction, there is little effect of switching the electric field as seen in Figs. 4(a)–4(f).

In summary, and by way of context setting for the triple dot case presented below, we have shown that the interplay between electric field and piezoelectric potential with an exciton in a single, self-assembled quantum dot is insufficient to induce spatial localization of the charge distribution in the plane perpendicular to applied field. This contrasts with the case of a single ring which does exhibit switching.[13]

2. Charge distribution in stacked dots: Lateral switching

In contrast to single dots, a stacked system made of two or three vertically stacked dots demonstrates the interesting phenomena of lateral switching of charge distribution as we now show.

In Fig. 5, the charge distribution of electron, hole, and exciton in a triple quantum dot is presented, in contrast with Fig. 4 for the single dot. In contrast to the single dot, the most striking feature of triple quantum system is a strong, diagonal localization of the charge distribution which we can accurately switch in the plane of the quantum dot by changing the direction of the perpendicular electric field, Figs. 5(a)–5(f). It is important to note that probability distribution in the top dot for the electron and the hole is 90° rotated with respect to the bottom one. This affects the picture and dilutes the sharp diagonal distribution. In fact we are looking down through all three quantum structures from the top, therefore, we see the residues of the distribution in middle and bottom quantum dots.

The much larger volume of alloy in the coupled structure compared to the single quantum dot induces a stronger piezoelectric potential. The piezoelectric field perturbs the confinement for the electron and hole, Figs. 3(c) and 3(d). An interesting characteristic of the triple dot system is that the piezoelectric field originating from the central dot is canceled by fields from the top and bottom structures. This leads to the symmetry along the [110] and $[1\bar{1}0]$ diagonals for the

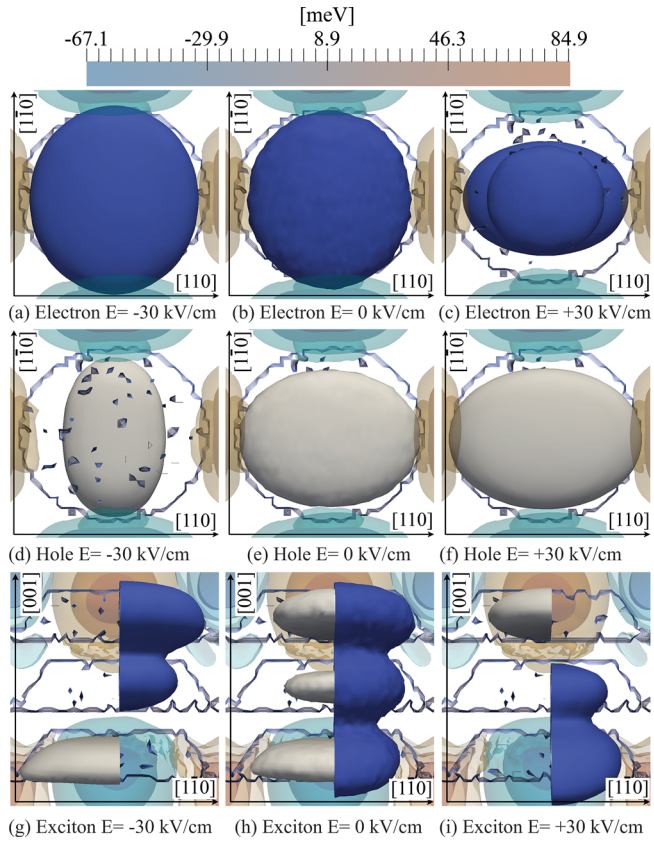

FIG. 5. Coupled quantum dot. Volumetric cross-section of electron and hole charge distributions with and without the applied vertical ([001]) electric field. We include isosurfaces of the piezoelectric potential and the outline of the quantum dot structure. In panels (a)–(f), the horizontal extent corresponds to the [110] direction and the vertical one to the $[1\bar{1}0]$ direction. In panels (g)–(i), the height of picture represents the [001] direction and the width $[1\bar{1}0]$ direction, and for clarity, the hole isosurface is shown on the left (grey) and electron isosurface on the right (blue).

middle dot. The piezoelectric potential penetrates into the top and bottom structures creating local minima and maxima in the dot confining potential, Figs. 3(c) and 3(d).

In Fig. 5(b), the top view of the electron charge probability distribution can be compared to the electron distribution in the vertical cross-section Fig. 5(h) in the absence of external electric field. We see strong delocalization of the electron probability density in the whole dot volume and uniformly in all three quantum dots. The hole charge distribution, however, is strongly confined to the central region of each of the dots, Fig. 5(e). In Fig. 5(h), it is also apparent that the hole charge distribution is shifted toward the base of each dot with highest probability to be found in top and bottom dots. As already indicated, the confinement differs in all three structures and also along diagonals in the plane of the dots. The top and bottom dots are characterized by deeper wells compared to the middle one. The repelling action of positive piezoelectric lobes and different strength of confinement on the diagonals naturally favors localization of the hole in an outer dot, as much more energy is required to overcome the barrier and transit to the central structure. This is clearly visible in Fig. 5(h).

B. Electron-hole pair correlation functions

Further insight into the electron-hole distribution in the single and coupled quantum dot systems can be obtained from the pair correlation function $g(r)$. In Fig. 6, the pair correlation data are plotted for the single and triple dot, with and without an electric field. We study two opposite directions of the electric field at ± 30 kV/cm. As before, we start with the single dot system without an electric field and compare it to the coupled structure. In Fig. 6(b), the pair correlation function (PCF) for the single and triple system is plotted in the absence of an electric field. The exciton in the single dot is strongly bound by the Coulomb interaction, and the particle separation is close to physical height of the structure. This separation can be slightly greater, as the electron is free to tunnel into the surrounding material, and the hole favors the wider bottom of the structure. An increase of the electric field pulls the exciton apart; this weakens the Coulomb interaction and confinement, allowing the charge distribution to spread across and even outside the dot.

The PCF of the triple dot structure, Fig. 6(b), shows some additional features not present in the single quantum dot. One can see two distinguishable maxima at 4 nm and 8 nm, Fig. 6(b). The first, lower maximum, corresponds to the spatially direct exciton when the particles occupy the same structure. The second one indicates the spatially indirect exciton when the electron and the hole occupy neighboring dots.

The application of a vertical electric field to the system affects the single and multiple structures in a completely different ways. The plot of the PCF, Fig. 6(a) for the single quantum dot hardly changes when the external field is applied. The strong confining potential of the structure keeps the exciton localized in the dot. The hole, which is much heavier than the electron, localizes towards the base of the quantum dot. The electron on the other hand is delocalized

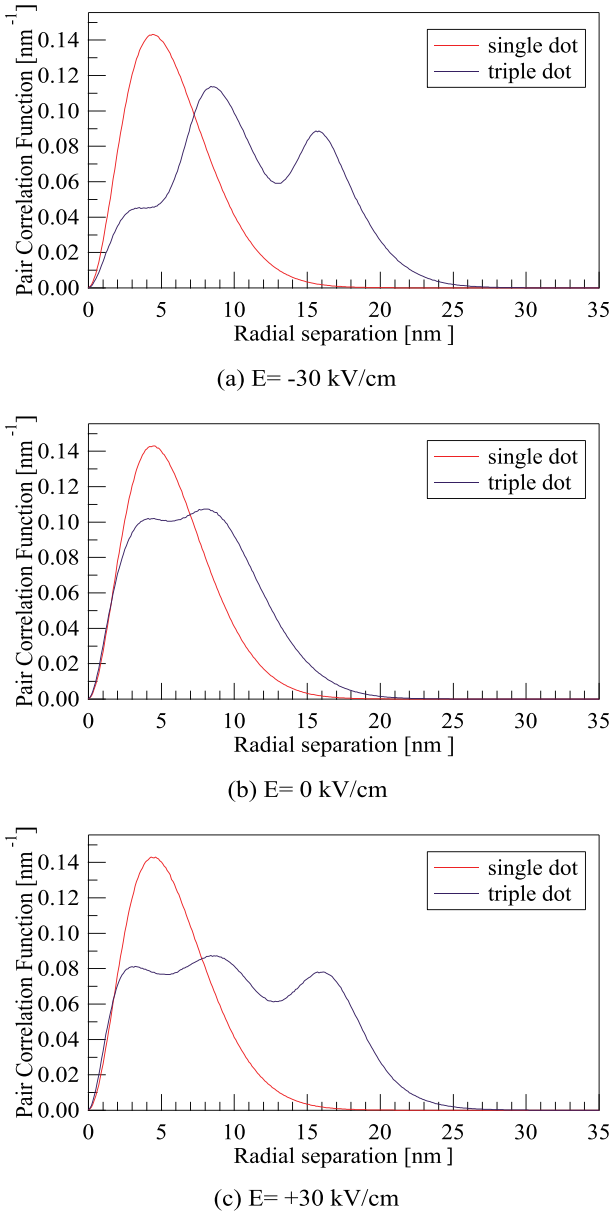

FIG. 6. Pair correlation function for the single and triple quantum dots for three electric field values.

in the whole structure, including tunnelling into the barrier material. The positive hole and the negative electron form the electric dipole. Application of an external electric field stretches/compresses the electron-hole pair in the vertical direction. Changing the orientation of the field flips the system's overall polarity, however, the electron-hole separation is only marginally affected.

The coupled quantum dots are far more sensitive to the change of environment compared to the single one, Fig. 6(a). We see that even small changes in an applied field yields substantial variations in the charges' relative position. For $E = +30$ kV/cm, the most energetically favorable configuration is the one in which the electron and hole are confined to neighboring dots. The charge carriers tunnel between the middle and outer quantum dots, however, the lowest to middle transition dominates. The electric field creates a dipole by stretching the exciton towards the top and base of

opposite dots, promoting inter-dot tunnelling. The electron and the hole tend to occupy neighboring structures, Fig. 6(c), in this case, the bottom and the middle dot (see Fig. 5(i)). When the sign of E is negative (Fig. 6(a)), the occupancy of the middle and top dots dominates.

In the above section, we have shown that an exact treatment of the electron-hole Coulomb potential, as well as a full description of the strain and piezoelectric fields, in the PI-QMC simulations, demonstrates that lateral switching, hitherto only predicted to occur in quantum rings, may also be found in stacked quantum dots. The charge distributions clearly demonstrate the switching between two perpendicular diagonals of the couple quantum dot systems in response to the change of orientation of the vertical electric field. This effect is absent in the single quantum dot due to the much weaker piezoelectric potential within the dot. The localized charge distribution functions for the electron and hole are in excellent agreement with the pair correlation results.

C. Lateral polarizability as a probe of switching

One possibility to measure the lateral switching effect described here would be to monitor the lateral polarizability of the quantum dot. This could be achieved, e.g., by use of surface contacts to apply a small fixed lateral electric field and monitor the shift in the photoluminescence as a function of this field. The shift will be proportional to the lateral polarizability hence will change with the exciton switch described earlier. This would be accompanied by an increase in the exciton lifetime as the electron and hole are separated (see Section IV D). The observation of these two effects at the same vertical field value would confirm the lateral switching. The second strong indicator of the lateral switching would be to observe a switching in the optical polarization of the photoluminescence emission, however, because of band-mixing effects, a quantitative estimate of the efficiency of such switching is beyond the single valence band calculations adopted here.

As the exciton transition goes from spatially direct to indirect, the oscillator strength varies for different values of the external field. Due to the different potentials on planes [110] and $[1\bar{1}0]$, the measured oscillator strength is not symmetric around the 0 kV/cm point, as the exciton is attracted by local minima and maxima in top and bottom structure in a different way. Changing the direction of the electric field in the vertical direction lowers the energy on one of the diagonals and promotes the lateral switching between the [110] and $[1\bar{1}0]$ directions, (Fig. 5). As a result, an increase in the lateral polarizability tangential to the direction of the confining potential is observed as shown in Fig. 7.

It is important to note that the lateral switch operates only for values of electric field in the range ± 30 kV/cm. Stronger fields, more than ± 40 kV/cm, break the exciton. The unbound charge carriers are then attracted and trapped by the piezoelectric extrema, and the lateral polarizability remains constant in the triple dot structure. Orientation of vertical electric field still swaps their spatial distribution in the coupled quantum dot, however, the lateral switching is not possible anymore, due to its Coulombic nature.

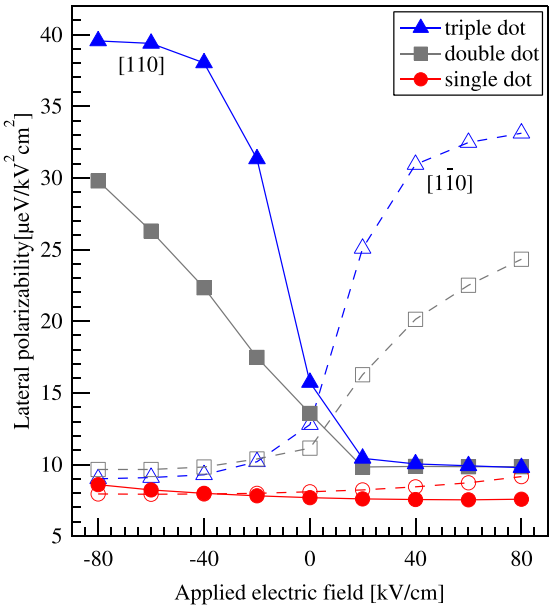

FIG. 7. Comparison of lateral polarizability calculations of excitons in the [110] and $[1\bar{1}0]$ direction versus applied vertical electric field for different heterostructures.

The situation is a little different in a double dot, in which the lateral switching is preserved even for higher values of an electric field. The smaller volume of the alloy in double dot creates a weaker piezoelectric potential which attracts the charges. The electron and the hole are able to tunnel between the top and bottom structures as the dots are relatively close. From a different point of view, a strong electric field tries to pull the electron-hole system apart and extend the electric dipole in the surroundings forcing it out of the structure. The sum of the piezoelectric and confining potentials is however strong enough to preserve the Coulomb interaction and sustain the lateral switching. When the orientation of the external electric field is changed, the polarizability in the $[1\bar{1}0]$ direction is much larger. It is clear, Fig. 7, that the response of the exciton to the electric field in a single dot is extremely weak compared to the multiple-dot structures. This is caused by the electron and the hole occupying of the same structure. The small vertical separation between the electron and the hole creates a much weaker dipole, which in addition is tightly bound by the confining potential of the single quantum dot, and is perturbed less by the associated weaker piezoelectric fields of the single dot. A coupled structure's bright states can be examined experimentally by measuring the lateral polarizability of the exciton, which determines the sensitivity of excitonic energy to an electric field, Fig. 7, and can be used to confirm the lateral switching phenomenon.

D. Effect of lateral switching on photoluminescence

We have also calculated the emission energy (Fig. 8) and radiative recombination rate (Fig. 9) of the single and triple dots. Such calculations are important as if the switched exciton is optically dark due to the spatial switching, detecting the switching phenomenon would be difficult.

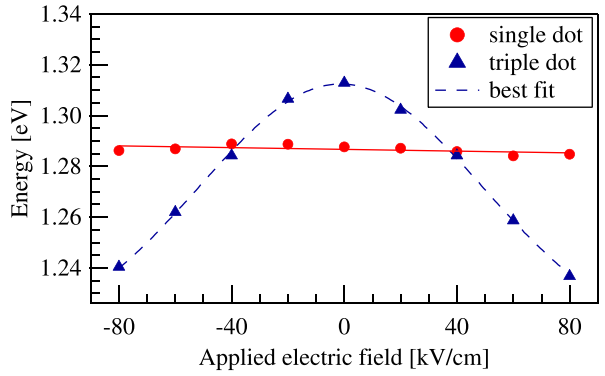

FIG. 8. Energy of PL emission for an exciton as a function of applied electric field in the growth direction in single and triple quantum dot.

In the single dot, the radiative recombination rate and the transition energy are rather insensitive to the applied field due to the strong confinement. In contrast with the triple dot, the electron-hole radiative recombination rate drops off as the applied field is increased and the exciton is essentially dark at fields higher than ± 40 kV/cm. For the stronger fields, e.g., ± 80 kV/cm, the fields overcome the Coulomb attraction splitting the exciton apart. At this point, the electron and hole occupy different structures, wave functions do not overlap any more, and the oscillator strength drops essentially to zero.

V. CONCLUSIONS

We have used path integral quantum Monte Carlo calculations to study a heavy-hole exciton in single and multiple quantum dots. We found that the lateral switching of the charge distribution in the vertical electric field, previously reported for quantum rings, is also clearly presented and highly tuneable in the system of stacked quantum dots. On the other hand, it cannot be observed in a single quantum dot structure. We have also investigated the lateral switching in dots of different shapes, sizes, and composition profiles. It was found that these generic phenomena are caused by the interplay of piezoelectric field deformation of conduction and valence bands and the coulomb interaction. Switching was observed for applied fields sufficiently small that exciton dissociation was not a factor hence an optical observation of this phenomenon should be feasible.

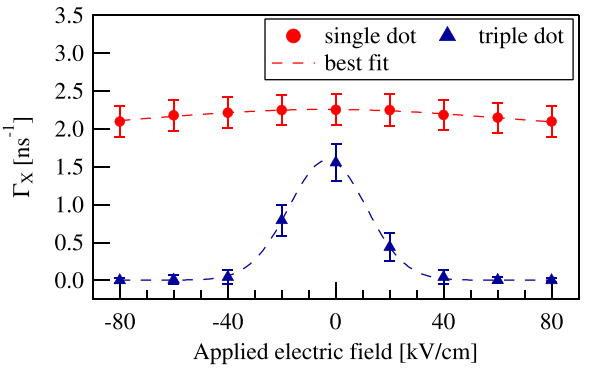

FIG. 9. Exciton recombination rates as a function of applied electric field in the vertical direction with the lines of best fit. The error bars arise from the statistical uncertainty of the PI-QMC calculation.

[1]P. Kómár, E. M. Kessler, M. Bishof, L. Jiang, A. S. Sørensen, J. Ye, and M. D. Lukin, "A quantum network of clocks," Nat. Phys. **10**(8), 582–587 (2014).
[2]H. J. Kimble, "The quantum internet," Nature **453**, 1023 (2008).
[3]G. Grosso, J. Graves, A. T. Hammack, A. A. High, L. V. Butov, M. Hanson, and A. C. Gossard, "Excitonic switches operating at around 100 K," Nat. Photonics **3**(10), 577–580 (2009).
[4]A. J. Shields, "Semiconductor quantum light sources," Nat. Photonics **1**(4), 215–223 (2007).
[5]K. De Greve, L. Yu, P. L. McMahon, J. S. Pelc, C. M. Natarajan, Na. Y. Kim, E. Abe, S. Maier, C. Schneider, M. Kamp, S. Hofling, R. H. Hadfield, A. Forchel, M. M. Fejer, and Y. Yamamoto, "Quantum-dot spin-photon entanglement via frequency down conversion to telecom wavelength," Nature **491**(7424), 421–425 (2012).
[6]P. Michler, A. Kiraz, C. Becher, W. V. Schoenfeld, P. M. Petroff, L. Zhang, E. Hu, and A. Imamoglu, "A quantum dot single-photon turnstile device," Science **290**(5500), 2282–2285 (2000).
[7]H. J. Krenner and P. M. Petroff, "Quantum posts with tailored structural, electronic and optical properties for optoelectronic and quantum electronic device applications," Solid State Commun. **149**(35–36), 1386–1394 (2009).
[8]Y. H. Huo, B. J. Witek, S. Kumar, J. R. Cardenas, J. X. Zhang, N. Akopian, R. Singh, E. Zallo, R. Grifone, D. Kriegner, R. Trotta, F. Ding, J. Stangl, V. Zwiller, G. Bester, A. Rastelli, and O. G. Schmidt, "A light-hole exciton in a quantum dot," Nat. Phys. **10**(1), 46–51 (2014).
[9]A. Schliwa, M. Winkelnkemper, and D. Bimberg, "Few-particle energies versus geometry and composition of In_x $Ga_{1-x}As$/GaAs self-organized quantum dots," Phys. Rev. B **79**, 075443 (2009).
[10]D. L. Huffaker, G. Park, Z. Zou, O. B. Shchekin, and D. G. Deppe, "1.3 μm room-temperature GaAs-based quantum-dot laser," Appl. Phys. Lett. **73**(18), 2564–2566 (1998).
[11]H. Cao, H. Deng, H. Ling, C. Liu, V. A. Smagley, R. B. Caldwell, G. A. Smolyakov, A. L. Gray, L. F. Lester, P. G. Eliseev, and M. Osiński, "Highly unidirectional InAs/InGaAs/GaAs quantum-dot ring lasers," Appl. Phys. Lett. **86**(20), 203117 (2005).
[12]A. Imamoglu, D. D. Awschalom, G. Burkard, D. P. DiVincenzo, D. Loss, M. Sherwin, and A. Small, "Quantum information processing using quantum dot spins and cavity qed," Phys. Rev. Lett. **83**, 4204–4207 (1999).
[13]P. G. McDonald, J. Shumway, and I. Galbraith, "Lateral spatial switching of excitons using vertical electric fields in semiconductor quantum rings," Appl. Phys. Lett. **97**(17), 173101 (2010).
[14]J. Shumway, A. J. Williamson, A. Zunger, A. Passaseo, M. DeGiorgi, R. Cingolani, M. Catalano, and P. Crozier, "Electronic structure consequences of In/Ga composition variations in self-assembled $In_xGa_{1-x}As$/GaAs alloy quantum dots," Phys. Rev. B **64**, 125302 (2001).
[15]P. N. Keating, "Effect of invariance requirements on the elastic strain energy of crystals with application to the diamond structure," Phys. Rev. **145**, 637–645 (1966).
[16]M. Harowitz, D. Shin, and J. Shumway, "Path-integral quantum Monte Carlo techniques for self-assembled quantum dots," J. Low Temp. Phys. **140**, 211–226 (2005).
[17]A. Beya-Wakata, P.-Y. Prodhomme, and G. Bester, "First- and second-order piezoelectricity in III-V semiconductors," Phys. Rev. B **84**, 195207 (2011).
[18]J. H. Davies, "Elastic and piezoelectric fields around a buried quantum dot: A simple picture," J. Appl. Phys. **84**, 1358–1365 (1998).
[19]"Basics of semiconductor and spin physics," in *Spin Physics in Semiconductors*, Springer Series in Solid-State Sciences **157**, edited by M. I. Dyakonov (Springer, Berlin, Heidelberg, 2008), pp. 1–28.
[20]A. Schliwa, M. Winkelnkemper, and D. Bimberg, "Impact of size, shape, and composition on piezoelectric effects and electronic properties of In(Ga)As/GaAs quantum dots," Phys. Rev. B **76**(20), 205324 (2007).
[21]R. J. Warburton, C. Schulhauser, D. Haft, C. Schäflein, K. Karrai, J. M. Garcia, W. Schoenfeld, and P. M. Petroff, "Giant permanent dipole moments of excitons in semiconductor nanostructures," Phys. Rev. B **65**(11), 113303 (2002).

[22]S. Raymond, J. P. Reynolds, J. L. Merz, S. Fafard, Y. Feng, and S. Charbonneau, "Asymmetric stark shift in $Al_xIn_{1-x}As/Al_yGa_{1-y}As$ self-assembled dots," Phys. Rev. B **58**, R13415–R13418 (1998).
[23]P. W. Fry, I. E. Itskevich, D. J. Mowbray, M. S. Skolnick, J. J. Finley, J. A. Barker, E. P. O'Reilly, L. R. Wilson, I. A. Larkin, P. A. Maksym, M. Hopkinson, M. Al-Khafaji, J. P. R. David, A. G. Cullis, G. Hill, and J. C. Clark, "Inverted electron-hole alignment in InAs/GaAs self-assembled quantum dots," Phys. Rev. Lett. **84**, 733–736 (2000).
[24]P. W. Fry, I. E. Itskevich, S. R. Parnell, J. J. Finley, L. R. Wilson, K. L. Schumacher, D. J. Mowbray, M. S. Skolnick, M. Al-Khafaji, A. G. Cullis, M. Hopkinson, J. C. Clark, and G. Hill, "Photocurrent spectroscopy of InAs/GaAs self-assembled quantum dots," Phys. Rev. B **62**, 16784–16791 (2000).
[25]J. A. Barker, R. J. Warburton, and E. P. O'Reilly, "Electron and hole wave functions in self-assembled quantum rings," Phys. Rev. B **69**(3), 035327 (2004).